AIAA-2000-4154

Robust Inversion and Data Compression in Control Allocation

A. Scottedward Hodel[1] [2]

Abstract

We present an off-line computational method for control allocation design. The control allocation function $\delta = F(z)\tau = \delta_0(z)$ mapping commanded body-frame torques to actuator commands is implicitly specified by trim condition $\delta_0(z)$ and by a robust pseudo-inverse problem

$$\|I - G(z)F(z)\| < \epsilon(z)$$

where $G(z)$ is a system Jacobian evaluated at operating point z, $\hat{z}$ is an estimate of z, and $\epsilon(z) < 1$ is a specified error tolerance. The allocation function $F(z) = \sum_i \psi_i(z)F_i$ is computed using a heuristic technique for selecting wavelet basis functions ψ and a constrained least-squares criterion for selecting the allocation matrices F_i. The method is applied to entry trajectory control allocation for a reusable launch vehicle (X-33).

1. Introduction

We consider control allocation design for a reusable launch vehicle (see Figure 1). The problem is described as follows. Let $\delta \in \mathbb{R}^m$ be a vector of actuator conditions (aerosurface positions, engine thrust vectoring, etc.) and let $z \in \mathbb{R}^n$ be a vector of vehicle operating conditions (angle of attack α, mach number M, etc.) such that the the controlled vehicle torques

$$\tau = \begin{bmatrix} \tau_x & \tau_y & \tau z \end{bmatrix}^T$$

τ may be described as $\tau = f_\tau(\delta, z)$ for some function f_τ. Let τ_c be a vector of controlled vehicle torques commanded by the attitude control system and let $\hat{z}$ be an estimate of vehicle operating conditions z. The *control allocation problem* is to design a control allocation law $\delta_c(\hat{z}, \tau_c)$ specifying actuator commands δ_c such that vehicle body torques $f_\tau(z, \delta_c(\hat{z}, \tau_c))$ match the commanded torques τ_c to within a specified tolerance.

We present an off-line computational approach for a gain scheduled linear affine control allocation law $\delta_c(z, \tau_c) = F(z)\tau_c + \delta_0(z)$ where $\delta_0(z)$ is a trim function selected such that $f_\tau(\delta_0(z), z) = 0$ and

$$F(z) \triangleq \sum_{i=1}^{n_\psi} \psi_i(z)F_i \qquad (1.1)$$

is a gain scheduled control allocation matrix computed from basis (wavelet) functions $\Psi = \{\psi_i\}_{i=1}^{n_\psi}$ and their corresponding weighting matrices $\mathcal{F} = \{F_i\}_{i=1}^{n_\psi}$.

2. Control Allocation Design

Let Ω be a region of operating points ($z \in \Omega$) and define

$$G(z) \triangleq \nabla_\delta f_\tau(\delta, z)|_{\delta=\delta_0(z)} : z \in \Omega$$

Ideally, the control allocation matrix $F(z)$ is selected to be a pseudo-inverse of $G(z)$,

$$G(z)F(z) = I.$$

However, lack of precise measurements of operating conditions z and actuator saturation issues can prevent achievement of this ideal condition.

The use of an estimate $\hat{z}$ for gain scheduling requires that we relax the above pseudo-inverse condition. Let $\epsilon_\tau(z)$ be a specified error tolerance defined

[1] Dept. Electrical and Computer Engineering, Auburn University. On leave at Marshall Space Flight Center

on $z \in \Omega$ and let $Q = Q^T \geq 0$ be a selected matrix to define a quadratic norm $\|z\|_Q = \frac{1}{2}\sqrt{z^T Q z}$. Then a revised control allocation performance condition may be written as

$$\|I - G(z)F(\hat{z})\| < \epsilon_\tau(z) : \|\hat{z} - z\|_Q \leq \epsilon_z \qquad (2.1)$$

We require $\epsilon_\tau(z) < 1$ since this condition guarantees $\tau^T \tau_c > 0$, i.e., the resulting controlled vehicle torques have "the correct sign," which is a necessary condition for several attitude control strategies ([5], [6]).

Actuator saturation issues may be dealt with in part by incorporating the constraint

$$\|W_\delta F(\hat{z}) W_\tau\| < 1, \hat{z} \in \Omega \qquad (2.2)$$

where W_δ and W_τ are weighting matrices selected based on actuator saturation limits and anticipated maximum torque command magnitudes, respectively. Notice that equation (2.2) is a convex constraint on the linear-affine matrix function $F(\hat{z})$.

In the absence of constraints (2.1) and (2.2), the ideal control allocation problem may be relaxed to a simple least-squares optimization

$$\min \int_{z \in \Omega} \int_{h:\|h\|_Q \leq \epsilon_z} \|I - G(z)F(z+h)\|^2 \, dh dz \qquad (2.3)$$

The use of constraints (2.1) and (2.2) yields a convex programming problem over $z, \hat{z}$.

We propose a candidate (off-line) solution procedure that iteratively selects a set of basis wavelet functions Ψ and a corresponding set of weighting matrices $\mathcal{F}$. Our candidate procedure assumes that the optimization (2.3) subject to constraints (2.1) and (2.2) is feasible; that is, there exist Ψ, $\mathcal{F}$ that satisfy the constraint conditions. The procedure is as follows.

Algorithm 2.1 Control allocation design procedure.

Inputs Target error tolerance function $\epsilon_\tau(z)$, system Jacobians $G(z)$, measurement uncertainty parameters $Q = Q^T \geq 0$ and $\epsilon_z > 0$.

Outputs Wavelet set Ψ and a corresponding set of weighting coefficient matrices $\mathcal{F}$ to specify the allocation function $F(z)$ per equation (1.1).

1. $k := -1$
2. **do**
   (a) $k := k + 1$
   (b) **if** $k = 0$ **then** select an initial set of candidate wavelets Ψ_0.
   (c) **else** Update Ψ_{k-1} to obtain a new set of candidate wavelets Ψ_k.
   (d) **end if**
   (e) Compute a set of matrices $\mathcal{F}_k$ corresponding to Ψ_k satisfying the minimization (2.3).
   (f) Define $F_k(z)$ from equation (1.1) for $\psi_i \in \Psi_k$, $F_i \in \mathcal{F}_k$
3. **until** F_k satisfies constraints (2.1) and (2.2).

Remark 2.1 Let

$$e_k = \max \|I - G(z)F(\hat{z})\| - \epsilon_\tau(z) : z, \hat{z} \in \Omega, \|z - \hat{z}\|_Q \leq \epsilon_z$$

The wavelet sets Ψ_k should be selected such that the sequence e_k is monotone decreasing. In principle, one may select the set of wavelets Φ_k so that they provide increased resolution at values of $z \in \Omega$ where the constraint (2.1) is violated by $F_{k-1}(z)$ corresponding to Φ_{k-1}, $\mathcal{F}_{k-1}$. By consequence, the updated wavelets provide additional degrees of freedom to the unconstrained optimization (2.3) so that the computed values $\mathcal{F}_k$ yield a function $F(z)$ that is "nearer" to a feasible solution to the constrained optimization.

3. Computational approach

We now consider Algorithm 2.1 in further detail. Since the function $f_\tau(z, \delta)$ is often available only in sampled form through, e.g., wind tunnel data, we select a set of N operating points $\mathcal{Z} = \{z_i\}_{i=1}^N \in \Omega$ in the operating region Ω. Associate with $\mathcal{Z}$ the set of Jacobians $\mathcal{G} = \{G_i = G(z_i), z_i \in \mathcal{Z}\}$. With the function $G(z)$ thus sampled, given a set of n_w wavelets $\Psi = \{\psi_i\}_{i=1}^{n_w}$, the unconstrained control allocation problem (2.3) becomes a matrix-valued (dense) least squares problem of the form

$$\min_X \|AX - B\|$$

where

$$X = \begin{bmatrix} F_1 \\ \vdots \\ F_{n_\omega} \end{bmatrix} \quad \text{and} \quad B = \begin{bmatrix} I \\ \vdots \\ I \end{bmatrix}$$

and each block-row $A_{i,\cdot}$ of A is of the form

$$\begin{bmatrix} \psi_1(z_j)G_i & \cdots & \psi_{n_\omega}(z_j)G_i \end{bmatrix} \qquad (3.1)$$

where $\|z_j - z_i\|_Q \leq \epsilon_z$, which may be solved readily through a QR-factorization [1]. Further, if the dimension of the minimization is not too large, recently developed convex programming techniques [3], [9] allow the norm constraint

$$\begin{aligned} \|I - G(z_i)F(\hat{z}_i)\| &< \epsilon_\tau(z) \\ &: \quad z_i, \hat{z}_i \in \mathcal{Z},\ \|\hat{z}_i - z_i\| \leq \epsilon_z \end{aligned}$$

to be directly included in Algorithm 2.1 step 2e. Should the dimension of the minimization (3.1) be too large for practical direct application of convex programming techniques, one may employ an iterative algorithm to update individually the matrix values $F_i \in \mathcal{F}_k$, holding the other unknowns fixed. More precisely, we may replace step 2e of Algorithm 2.1 with the following procedure.

Algorithm 3.1 Tune weighting matrices

1. Compute $\mathcal{F}_k$ from the unconstrained least squares minimization (3.1).
2. **for each** wavelet $\psi_j^{(k)} \in \Psi_k$
   (a) Identify sample points $z_j \in \Omega$ contained in the support of $\psi_i^{(k)}$.
   (b) Select weights $c_1, c_2 > 0$ and update the weighting matrix $F_i^{(k)} \in \mathcal{F}_k$ to solve

$$\begin{aligned} \min \quad & c_1 g + c_2 t \\ \text{subject to} \quad & \|I - G(z_j)F(\hat{z}_j)\| \\ & \quad < \epsilon_\tau(z) + g \\ & \|W_\delta F(z_j) W_\tau\| < 1 + t \end{aligned}$$

3. **end for**

Since the wavelets $\psi_i \in \Psi$ are assumed to be of finite support, for wavelets of higher degrees of resolution this reduces not only the column dimension of A but also its row dimension, and allows the incorporation of the norm constraint (see equation (2.1)) without undue increase of computational complexity.

Remark 3.1 Notice that Step 2b above does not directly enforce the constraints (2.1) and (2.2), but rather induces a trade-off between them in the computation. This is done to ensure feasibility of the posed convex optimization problem. Algorithm behavior may be tuned as needed by adjustment of selected coefficients c_1, c_2 or by adding other convex constraints, e.g., $g > 0$, as needed.

3.1. Wavelet decomposition

Formal development of a wavelet decomposition of a general function $F(z)$ [7] involves wavelet normalization and the definition of a multidimensional filter bank. Because the function $F(z)$ is only implicitly defined by the error criteria (2.1) and (2.3), the structure of the control allocation problem does not readily allow exploitation of wavelet properties of (bi-)orthogonality, etc., nor does does it admit direct application of a subset selection algorithm [2]. Reeves' Backward Greedy Algorithm [4] may be applied to the unconstrained problem (3.1), but this approach does not make use of the finite-support property of the set of wavelets Ψ, nor does it readily admit inclusion of the norm constraint (2.1) restricted to the set of operating points $\mathcal{Z}$.

For our purposes, it suffices to develop a heuristic algorithm to identify a small set of wavelet basis functions $\{\psi_i\}_{i=1}^{n_\omega}$ such that the error tolerance (2.1) can be achieved. For clarity in exposition, we shall use two-dimensional wavelets $\psi(x, y)$ where $\begin{bmatrix} x \\ y \end{bmatrix} = \Gamma z$ is a vector drawn from a 2-D hyperplane in $\mathbb{R}^n$. (Extension of our technique to higher dimensions is not difficult, but rapidly increases the computational complexity of the problem in terms of both off-line computation time and required storage in flight software.) We select the set of two-dimensional wavelets

$$\psi^{(ijk\ell)}(x, y) \triangleq \min\left(\psi^{(ij)}(x), \psi^{(k\ell)}(y)\right)$$

where i, j, k, ℓ are integers,

$$\psi^{(ij)}(x) \triangleq \psi(2^{-}i(x - j)).$$

and $\psi(\cdot)$ is the mother wavelet function (see Figure 2)

$$\psi(x) : \mathbb{R} \to \mathbb{R} : x \to \begin{cases} x+1 & x \in [-1,0] \\ 1-x & x \in [0,1] \\ 0 & \text{else} \end{cases}$$

(Notice that we do not normalize $\|\psi^{(ijk\ell)}\| = 1$; justification for this will be seen Algorithm 3.2 in the next subsection.) This class of wavelet basis functions may alternatively be interpreted as a Sugeno-Takagi fuzzy logic (STFL) function or as a first-order finite element solution; the use of convex programming in STFL based dynamic control for a fixed set of basis functions Ψ is addressed in [8]. We will occasionally write $F(x,y)$ rather than $F(z)$.

3.2. Selection of wavelets

Since the matrix values $\mathcal{F} = \{F_i\}_{i=1}^{n_w}$ are easily computed as the solution of a linear least-squares problem, we consider now the selection of the set of basis wavelet functions $\{\psi_i\}_{i=1}^{n_w}$ and its cardinality n_w. We select the sequence of wavelet sets Ψ_k in Algorithm 2.1 in an iterative process of subdividing two-dimensional wavelets $\psi^{(ijk\ell)}(x,y)$ with low index values i and k into "higher frequency" wavelets. We shall make use of the following terms:

Definition 3.1 Consider an arbitrary wavelet $\bar{\psi}(x,y) = \psi^{(ijk\ell)}(x,y)$.

1. The *center* of $\bar{\psi}$ is the point
$$(\bar{x},\bar{y}) = (j2^{-i}, \ell 2^{-k})$$
at which the wavelet has its maximum value.

2. The *$x-$axis children* of $\bar{\psi}(x,y)$ are the wavelets $\{\psi^{(i+1,j',k,\ell)}\}$ with $j' = 2j-1, 2j, 2j+1$. Notice that the support of the wavelet $\bar{\psi}$ is the union of the support of its $x-$axis children. Similarly, the *$y-$axis children* of $\bar{\psi}(x,y)$ are $\{\psi^{(i,j,k+1,\ell')}\}$ with $\ell' = 2\ell-1, 2\ell, 2\ell+1$. The support of the wavelet $\bar{\psi}$ is the union of the support of its $y-$axis children.

3. We say that a wavelet $\psi^{(ijk\ell)}(x,y)$ has *uniform resolution* in both axes if $i = k$. If $\bar{\psi}$ has uniform resolution we say that its *resolution level* is i.

4. Suppose that $\bar{\psi}$ has uniform resolution. Its *uniform resolution child wavelets*, or simply its *children*, are the $x-$axis children of its $y-$axis children (or, equivalently, the $y-$axis children of its *$x-axis$* children) whose centers are contained in the region Ω. Each wavelet has up to nine children.

5. Consider a set of wavelets Ψ with uniform resolution. The wavelet $\bar{\psi}$ with resolution level i is *redundant with* Ψ if (1) $\bar{\psi} \in \Psi$, or (2) its children are all redundant with Ψ. Alternatively, $\bar{\psi}$ is redundant with Ψ if the support of $\bar{\psi}$ can be written as the union of the supports of wavelets in a set $\Psi' \subseteq \Psi$ whose resolution level exceeds i.

We now present a refined version of Algorithm 2.1. Consider the N sample points $\mathcal{Z} = \{z_j\}_{j=1}^{N} \in \Omega$. Assume without loss of generality that $\Omega = [0,1] \times [0,1]$.

Algorithm 3.2 Control allocation design procedure

1. $k = 0$; Ψ_0 is selected to be the $2^p = 4$ basis wavelets with resolution level 0 centered at the vertices of Ω,
$$\begin{aligned} \Psi_1 &= \{\psi_1^{(0)}(x,y), ..., \psi_4^{(0)}(x,y)\} \\ &= \{\psi^{(0,0,0,0)}, \psi^{(0,0,0,1)}, \psi^{(0,1,0,0)}, \\ &\quad \psi^{(0,1,0,1)}\}. \end{aligned}$$

2. Compute a set of matrices $\mathcal{F}_0$ corresponding to Ψ_0 satisfying the minimization (3.1).

3. Define $F_0(z)$ from equation (1.1) for $\psi_i \in \Psi_0$, $F_i \in \mathcal{F}_0$

4. **while** F_k does not satisfy the constraint
$$\begin{aligned} \|I - G(z_i)F(\hat{z}_i)\| &< \epsilon_\tau(z) \\ &: \quad z_i, \hat{z}_i \in \mathcal{Z}, \\ &\qquad \|\hat{z}_i - z_i\| \le \epsilon_z \end{aligned}$$

   (a) Compute the error surface
$$\begin{aligned} \bar{e}_k(z_i) &= \max \|I - G(z_i)F(\hat{z})\| \\ &\qquad -\epsilon_\tau(z_i) \\ &: \quad z_i, \hat{z}_i \in \mathcal{Z}, \|z_i - \hat{z}_i\| \le \epsilon_z \end{aligned}$$
   and define $e_k(z_i) = \max\{0, \bar{e}_k(z_i)\}$.

(b) Identify a wavelet $\bar{\psi} \in \Psi_k$ with maximal inner product with the error surface e_k.

(c) $k := k + 1$

(d) Construct Ψ_k from Ψ_{k-1} by replacing $\bar{\psi}$ with its children.

(e) Define $F_k(z)$ from equation (1.1) for $\psi_i \in \Psi_k$, $F_i \in \mathcal{F}_k$

5. **end while**

Remark 3.2 Notice that e_k is nonnegative at all $z_i \in \mathcal{Z}$ and is positive only at points $z_i \in \mathcal{Z}$ where the norm constraint (2.1) is not met. $\langle \psi^{(ijk\ell)}, e_k \rangle \equiv 0 \Rightarrow$ the constraint (2.1) is met at all points z_i in the support of $\psi^{(ijk\ell)}$

Remark 3.3 Since the wavelets $\psi^{(ijk\ell)}$ are not normalized to have unit energy, the inner product criterion in step 4b is biased toward subdividing low-resolution wavelets. This heuristic process of subdivision quickly increases the level of resolution in those areas of Ω where it is needed while using low resolution levels where possible, reducing the computational requirements of the final control allocation flight code.

4. Design Example

We illustrate our design procedure in application to the X-33 experimental technology vehicle entry trajectory control allocation design. From the X-33 main engine cut off (MECO) to its target area energy management (TAEM) interface, the X-33 actuators include two pairs of elevons (left, right; outboard, inboard) and two body flaps (left, right). The left and right elevon pairs operate as a unit so that there are four deflection commands (left elevon, right elevon, left body flap, right body flap), $\delta_c \in \mathbb{R}^4$. Due to details of the vehicle, the trim deflection function for the $X-33$ is selected as

$$\delta_0(x) = \begin{bmatrix} \delta_{\text{left elevon}} \\ \delta_{\text{right elevon}} \\ \delta_{\text{left flap}} \\ \delta_{\text{right flap}} \end{bmatrix} = \begin{bmatrix} \delta_e \\ \delta_e \\ f_t(z) \\ f_t(z) \end{bmatrix}$$

where δ_e is a (constant) elevon bias position and $f_t(z)$ is a scalar-valued flap pitch trim function. (Roll and yaw torques resulting from $\delta_0(z)$ are all zero.) A set of eight reaction control system (RCS) thrusters are also available for entry maneuvers; for simplicity (and due to details of RCS thruster operation) these are neglected in this study.

The control allocation is scheduled on the angle of attack α and the Mach number M. 3-DOF simulations and dispersion (Monte Carlo) runs indicate that the range of these values is $\alpha \in [10°, 45°]$ and $M \in [3, 10]$. For the purposes of wavelet decomposition these ranges were normalized to $\Omega = [0, 1] \times [0, 1]$. A set of 1024 operating points $z_j \in \Omega$ were selected by superimposing an evenly spaced 32×32 rectangular mesh on the above intervals. A plot of condition $\kappa(G(z))$ of the Jacobian $G(z)$ from the surface deflections δ to body torques τ at trim conditions is shown in Figure 3. Based on the data in Figure 3 and other analysis of achievable performance, the target tolerance $\epsilon_\tau(z)$ was selected as shown in Figure as shown in Figure 4 with values between 0.5 and 0.71. The initial thresholded error surface e_1 for $n_w = 4$ is shown in Figure Figure 5. Two iterations later ($k = 3$) there are a total of $n_w = 9$ wavelets in Ψ_3 and the error surface e_3 is as shown in Figure 6; notice the decrease in maximum error above threshold and in the portion of Ω that meets the error criterion (2.1) (points at which $e_3 = 0$). The target tolerance $\epsilon_\tau(z)$ was achieved after a total of four iterations with a total of $n_w = 14$ wavelets in the database; a plot of $\max_j \psi_j^{(4)}(z)$ for $\psi_j^{(4)} \in \Psi_4$ is shown in Figure 7; peaks in the plot correspond to the centers of wavelet functions. (Use of least-squares optimization without re-tuning individual weights as in Algorithm 3.1 required $n_w = 53$ wavelets to achieve similar performance.)

The computed control allocation function $F(z)$ was tested in open-loop simulation by commanding a sawtooth wave in roll, pitch, and yaw torques (see Figures 8– 10). Torque command channels are coupled, but have acceptable performance as shown in the Figures. Aerosurface deflections (with ideal pitch trim function $\delta_0(z)$) are shown in Figure 11.

5. Conclusions

The design of control allocation for tail-less, lifting body reusable launch vehicles requires both ro-

bustness to measurement and modeling uncertainty and a computationally feasible implementation. We propose the off-line computation of a wavelet-based decomposition of an implicitly specified control allocation function

$$F(x) = \sum_i \psi_i(z) F_i + \delta_0(z)$$

We select piecewise linear wavelets through an iterative subdivision process in order to meet a maximum error criterion. The matrix weights $\{F_i\}$ are computed through the solution of a linear least squares problem. The method was applied to entry trajectory control allocation for the X-33 technology testbed and appears promising.

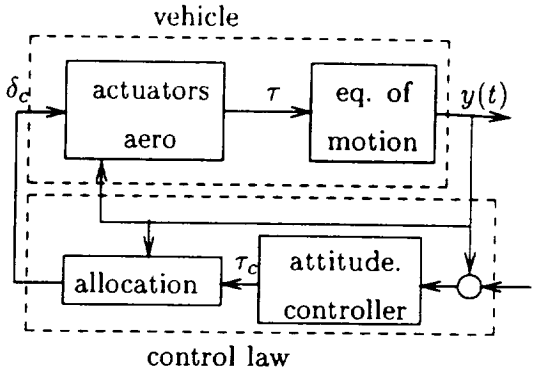

Figure 1: Block diagram of control allocation problem. It is desired to develop a set of control deflection commands δ_c such that the resulting body torques τ are "near" to the commanded body torques τ_c.

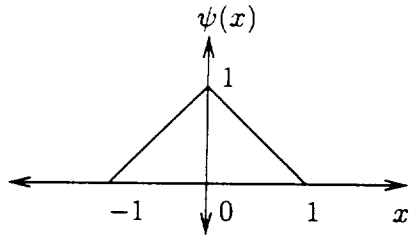

Figure 2: 1-D piecewise linear mother wavelet.

References

[1] G. H. Golub and C. Van Loan. *Matrix Computations*. Johns Hopkins University Press, Baltimore, MD, 2nd edition, 1989.

[2] Mohammed Nafie, Ahmed H. Tewfik, and Murtaza Ali. Deterministic and iterative solutions to subset selection problems. Manuscript, 2000.

[3] Yurii Nesterov and Arkadii Nemirovskii. *Interior-Point Polynomial Algorithms in Convex Programming*. SIAM, 1994.

[4] Stanley J. Reeves. An efficient implementation of the backward greedy algorithm for sparse signal reconstruction. *IEEE Signal Processing Letters*, 6(10):266–268, October 1999.

[5] Y. Shtessel, J. Buffington, and S. Banda. Multiple time scale flight control using reconfigurable sliding modes. *AIAA Journal on Guidance, Control, and Dynamics*, 22(6):873–883, 1999.

[6] Y. Shtessel, J. McDuffie, M. Jackson, C. Hall, D. Krupp, M. Gallaher, and N. Hentrix. Sliding mode control of the x33 vehicle in launch and reentry modes. In *Proceedings of AIAA Guidance, Navigation, and Control Conference*, number 98-4414, pages 1352–1362, Boston, MA, August 10-12 1998. AIAA.

[7] Gilbert Strang and Truong Nguyen. *Wavelets and Filter Banks*. Wellesley Cambridge Press, wellesley, mass. edition, 1996.

[8] K. Tanaka, T. Ikedo, and H. O. Wang. Robust stabilization of a class of uncertain nonlinear systems via fuzzy control: Quadratic stabilizability, $\mathcal{H}^\infty$ control. *IEEE Trans. Fuzzy Systems*, 4(1):1–13, 1996.

[9] Lieven Vandenberghe, Stephen Boyd, and Brien Alkire. . SP version 1.1 software for semidefinite programming. `http://www.ee.ucla.edu/~vandenbe/sp.html`, 1999.

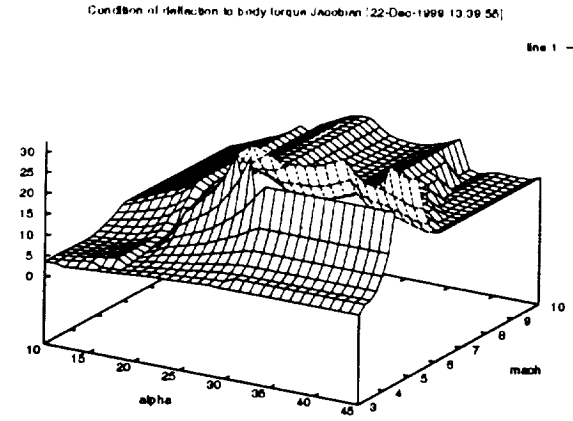

Figure 3: Pointwise condition number of the deflection to body torque Jacobian matrix $G(\alpha, M)$. Omitted values rapidly rise to a condition number $\kappa\left(G(\alpha, M)\right) \approx 160$. Corresponding values of G show less than 1% of yaw authority than that available in the pitch and roll channels. Mean and standard deviation of the condition number values shown in the plot are both approximately 15.

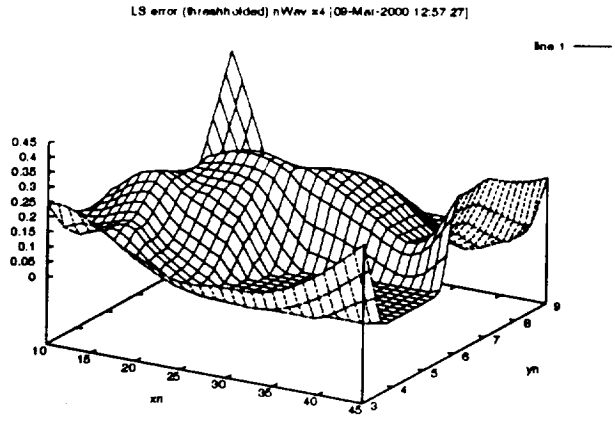

Figure 5: Initial error thresholded by target tolerance value

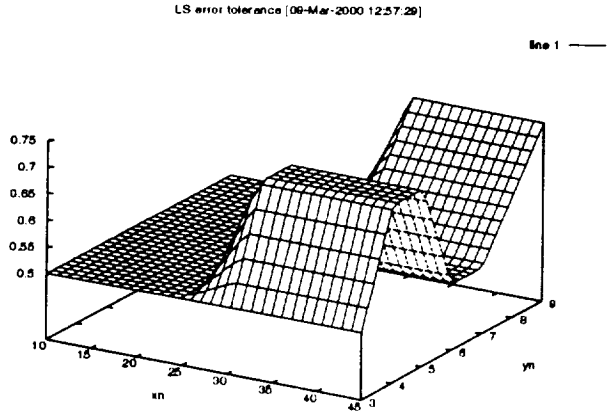

Figure 4: Maximum error tolerance for control allocation matrix computation

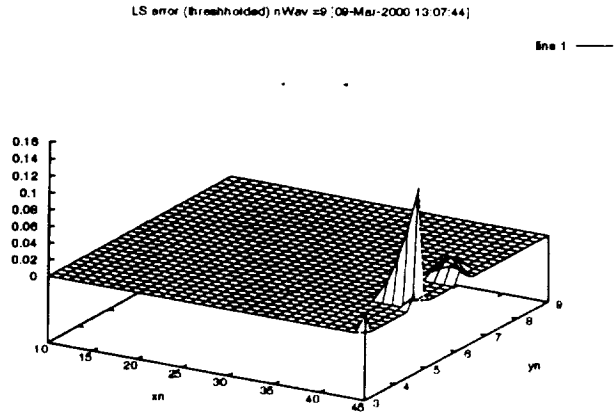

Figure 6: Threshold error surface after two iterations of wavelet subdivision.

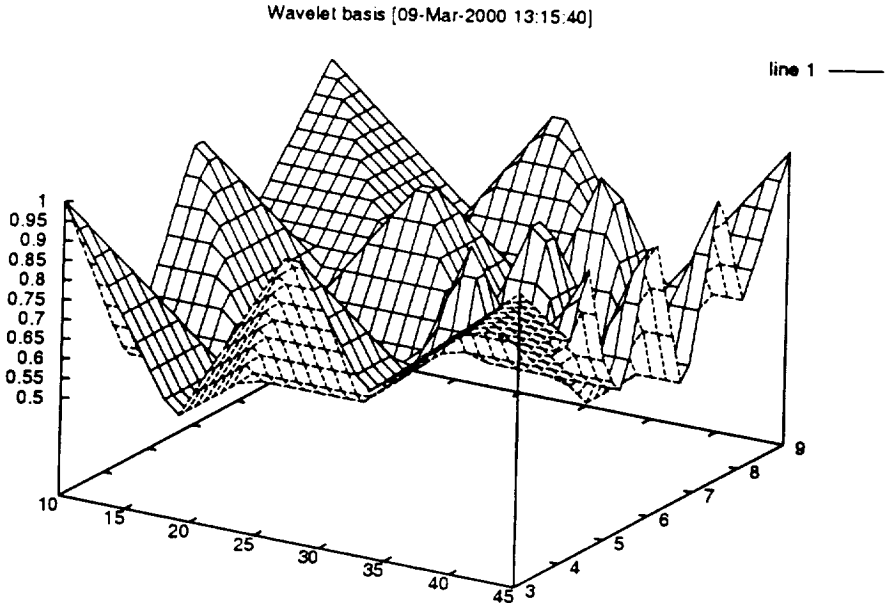

Figure 7: $\max_j \psi_j(z)$ for wavelet basis functions ψ_j selected for control allocation function $F(z)$.

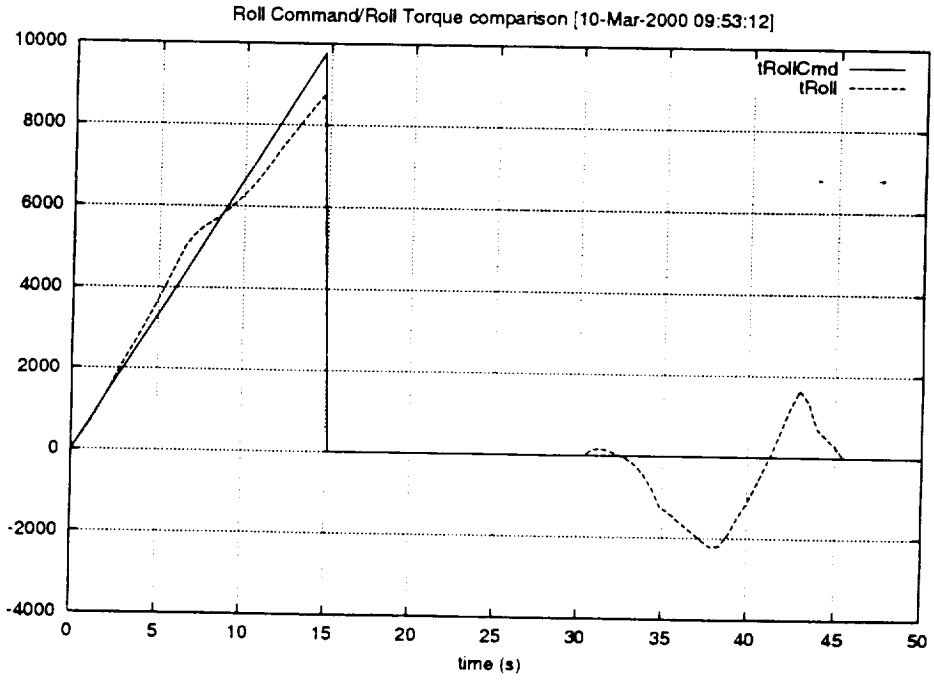

Figure 8: Control allocation test in simulation: roll command torque τ_c and body torque τ.

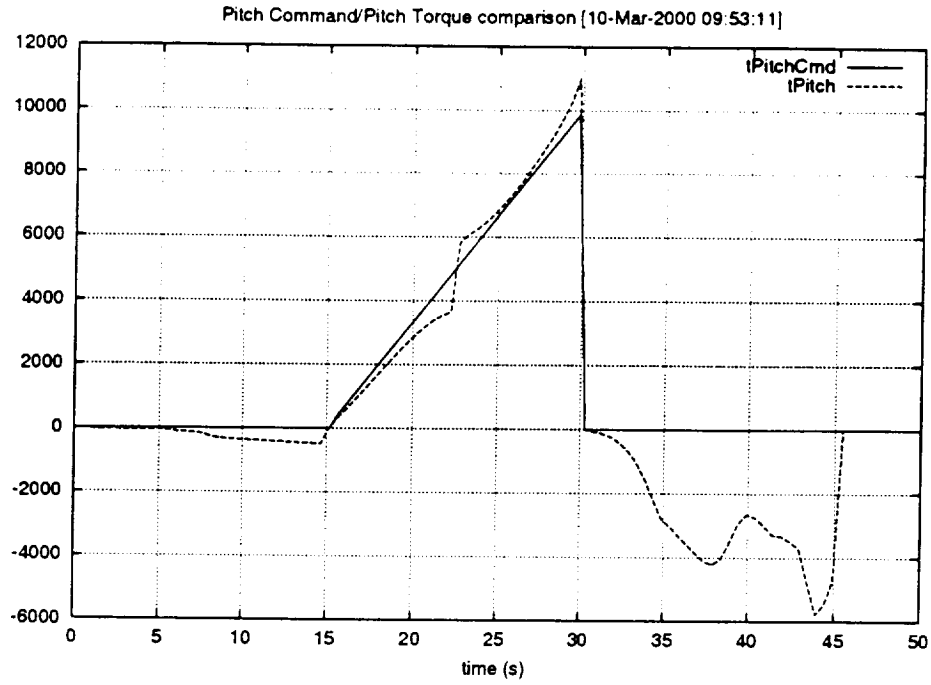

Figure 9: pitchtorque

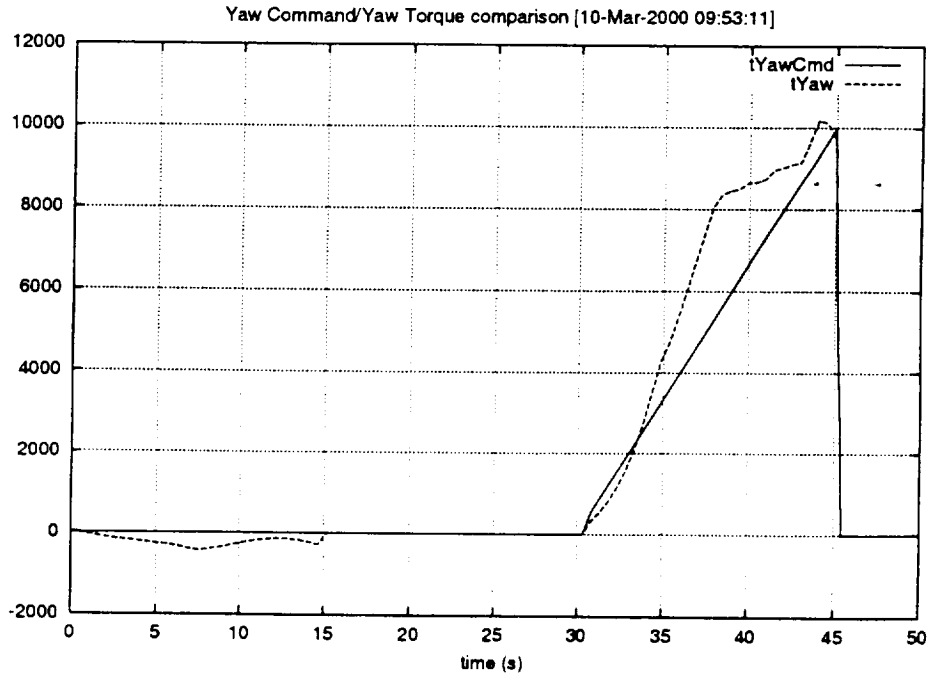

Figure 10: Control allocation test in simulation: yaw command torque τ_c and body torque τ.

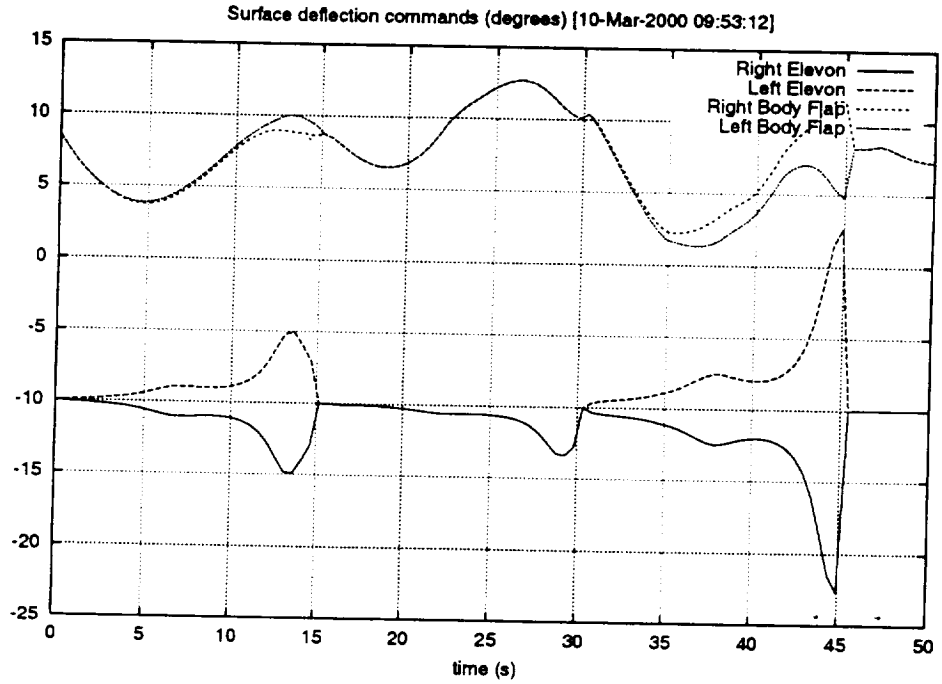

Figure 11: Control allocation test in simulation: aerosurface deflections with ideal pitch trim $\delta_0(z)$